

Progressive Confident Masking Attention Network for Audio-Visual Segmentation

Yuxuan Wang*, Feng Dong*, Jinchao Zhu†

Abstract—Audio and visual signals typically occur simultaneously, and humans possess an innate ability to correlate and synchronize information from these two modalities. Recently, a challenging problem known as Audio-Visual Segmentation (AVS) has emerged, intending to produce segmentation maps for sounding objects within a scene. However, the methods proposed so far have not sufficiently integrated audio and visual information, and the computational costs have been extremely high. Additionally, the outputs of different stages have not been fully utilized. To facilitate this research, we introduce a novel Progressive Confident Masking Attention Network (PMCANet). It leverages attention mechanisms to uncover the intrinsic correlations between audio signals and visual frames. Furthermore, we design an efficient and effective cross-attention module to enhance semantic perception by selecting query tokens. This selection is determined through confidence-driven units based on the network’s multi-stage predictive outputs. Experiments demonstrate that our network outperforms other AVS methods while requiring less computational resources.

Index Terms—audio-visual segmentation, cross-modal attention mechanism, dynamic network, multi-modality

I. INTRODUCTION

HUMANS perceive the world through multiple sensory modalities, including vision, hearing, tactile sense, taste, and smell. Recently, there has been a significant shift from single-modality [1] [2] [3] to multi-modality [4] [5] [6] [7] learning, which aims to enhance machine perception capabilities. One of the most common approaches involves integrating audio and visual information, leading to extensive research on audio-visual multi-modal learning methods. Unlike homogeneous multi-modalities in computer vision, such as RGB-Depth (RGB-D) [4] and RGB-Thermal (RGB-T) [5] [6], audio-vision is considered a heterogeneous multi-modality. Although these modalities do not share the same distribution, there exist intrinsic correlations between them. For instance, when hearing a guitar sound, one might expect to see a person holding a guitar in the scene rather than someone sitting in front of a piano. This is because humans can capture auditory and visual cues and simultaneously synthesize the information within their brains. However, integrating heterogeneous data poses significant challenges for neural network construction, making it crucial to explore new models in this area of research.

Y. Wang is with Department of Computing, Imperial College London. (e-mail: yuxuan.wang123@imperial.ac.uk).

Y. Wang, J. Zhu, and F. Dong are with Department of Automation, BNRIST, Tsinghua University. (e-mail: jczhu@mail.nankai.edu.cn).

J. Zhu and F. Dong are with College of Artificial Intelligence, Nankai University. (e-mail: jczhu@mail.nankai.edu.cn).

* equal contribution

† corresponding author

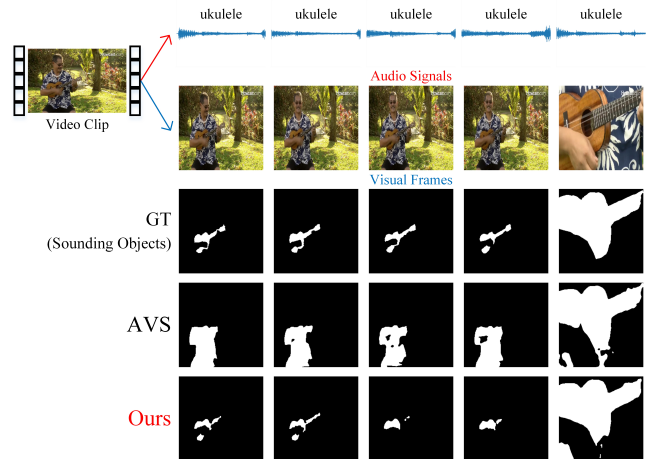


Fig. 1. An example of the audio-visual segmentation task (S4 dataset). The video depicts a man playing the glockenspiel. Within the clip, only the glockenspiel is sounding therefore it is the only object that is labeled.

In previous years, several audio-visual tasks have been proposed to enhance multi-modal perception abilities. With the advent of the big data era, millions of videos are uploaded to various applications daily, amounting to millions of hours of content in total. This has led to rapid growth in audio-visual learning, as videos serve as well-synchronized audio-visual pairs and can alleviate the need for extensive manual human labeling. Zhu *et al.* [8] categorized discriminative audio-visual tasks into three categories: 1) separation and localization, 2) corresponding learning, and 3) representation learning. For instance, a typical audio-visual task is Audio-Visual Correspondence (AVC) [9], [10], [11], [12], which aims to determine whether an audio signal and a video clip correspond or match each other. Another related task is Audio-Visual Event Localization (AVEL), which involves the temporal detection and localization of events within visual scenes [13], [14], [15], [16], [17].

As mentioned earlier, the number of unlabeled videos is rapidly increasing. Research on these tasks primarily focuses on semi-supervised learning [18] and unsupervised learning, particularly self-supervised learning [19], [20], [21], [22], [23], [24]. However, due to the lack of patch-level or pixel-level annotation, namely, supervision, these tasks are limited to image-level classification, and their applications are severely constrained. For years, researchers did not pay much attention to supervised learning and pixel-level annotation. Zhou *et al.* [25], [26] were the first to propose the Audio-Visual Segmentation (AVS) task and Audio-Visual Segmentation with

Semantic (AVSS) task, providing benchmark datasets specifically for these tasks. There is a similar task called Sound Source Localization (SSL) [20], [18], [21], [27], [22], [23], [28], [29], which aims to locate the regions in the visual scene that are relevant to the audio signals. Although it is not pixel-level, it is annotated at the patch-level. The results are typically represented by heat maps, which are obtained through similarity matrices or Class Activation Mapping (CAM) [30].

In this paper, our main focus is on the audio-visual segmentation problem, including audio-visual semantic segmentation. Figure 1 illustrates an example of the AVS task. Although significant progress has been made in previous works, three issues remain unresolved: 1. how to better integrate audio-visual features, 2. how to conserve computational resources, and 3. how to fully leverage multi-stage outputs. We propose a novel deep neural network architecture called Progressive Confident Masking Attention Network (PCMANet). The network follows the standard encoder-decoder architecture and consists of four major components. We introduce an Audio-Visual Grouped Attention (AVGA) module to intuitively emphasize the visual parts that correspond to the audio signals. To further integrate multi-modal information, we utilize a cross-attention mechanism with a specific design to reduce computational cost while retaining the most critical information. We name this mechanism Query-Selected Cross-Attention (QSCA). The selection process involves generating queries using only a few tokens while masking others. This encourages the network to focus on pixels that lack confidence, resulting in reduced computational costs. The confidence level of each pixel is determined by the Confidence-Induced Masking (CIM) unit, which generates masks based on the phased output maps. These masks are propagated from deep stages to the shallower stages. Finally, the Guided Fusion (GF) module combines the guiding signal and features from adjacent stages to generate segmentation prediction maps. Comprehensive experiments and visualization results demonstrate the effectiveness and reasonableness of the proposed models.

Our contributions can be summarized as follows:

- We propose an effective and efficient neural network called Progressive Confident Masking Attention Network (PCMANet) for the audio-visual segmentation task.
- We introduce an effective Audio-Visual Grouped Attention (AVGA) module to directly emphasize the visual region related to the audio signals. A novel audio-visual Query-Selected Cross-Attention (QSCA) using a considerably small number of tokens to calculate query. The selection mask is generated through a progressive Confidence-Induced Masking (CIM) unit.
- Experiments conducted on 3 audio-visual segmentation datasets illustrate that our model performs favorably against other state-of-the-art algorithms with relatively small computational costs.

II. RELATED WORK

A. Audio-Visual Correspondence

Audio-Visual Correspondence (AVC) is a critical task that aims to determine the relationship between audio snippets

and video frames to identify whether they originate from the same video clip. In recent years, several approaches have been proposed to improve the performance of the AVC task. Arandjelovic *et al.* [9] proposed the L3Net which contains visual, and audio subnetworks and the fusion network. To further enhance the alignment of audio and visual information, the scholars developed AVENet [10], which produces aligned vision and audio embeddings as the only information source. Owens *et al.* [11] utilized the 3D CNN with an early-fusion design to predict whether video frames and audio are temporally aligned. Korbar *et al.* [12] introduced another proxy task called Audio-Visual Temporal Synchronization (AVTS) that further considers whether a given audio sample and video clip are synchronized or not.

B. Sound Source Localization

Sound source localization (SSL) is quite similar to audio-visual segmentation. It aims to localize the regions and directions in the frames corresponding to the audio (the sound source). Senocak *et al.* [18] designed a two-stream network to compute the localization response by incorporating unsupervised video with a supervised loss to empower the network with prior knowledge. Cheng *et al.* [21] proposed a co-attention method employing cross-modal attention followed by self attention to learn the relationship between the audio and visual information. Chen *et al.* [28] introduced an automatic background mining technique and a Tri-map into the training procedure. Mo *et al.* [29] presented EZ-VSL, an effective multiple-instance learning framework, and proposed an object-guided localization scheme. Qian *et al.* [27] utilized a two-stage learning strategy, employing a multi-task framework for classification and correspondence learning, followed by Grad-CAM [31] to generate the localization map. Afouras *et al.* [22] designed LWTNet to use synchronization cues to detect sound sources and group them into distinct instances.

SSL is useful in many applications such as heading aids, television broadcasts, virtual reality, etc. But it doesn't have pixel-level prediction capability.

C. Audio-Visual Attention

The attention mechanism is widely used in audio-visual tasks. Various prior works have shown its effectiveness in audio-visual learning. Xuan *et al.* [16] designed a spatial, sequential, and cross-modal adaptive attention module to capture most event-related information. Wu *et al.* [14] utilized a dual attention matching module to model the high-level event information while capturing local temporal information by a global cross-check mechanism. Iashin *et al.* [32] proposed a Bi-modal Transformer followed by a multi-headed proposal generator to generate captions. Lin *et al.* [24] introduced a framework that learns the shared semantics through the audio and visual data across different videos and developed an audio-visual event co-occurrence module to consider the relationship of categories in audio-visual modalities. Lin *et al.* [17] designed an audiovisual-Transformer to jointly encode the intra-frame and inter-frame audio-visual context. Nagrani *et al.* [33] proposed a new architecture called MBT, which

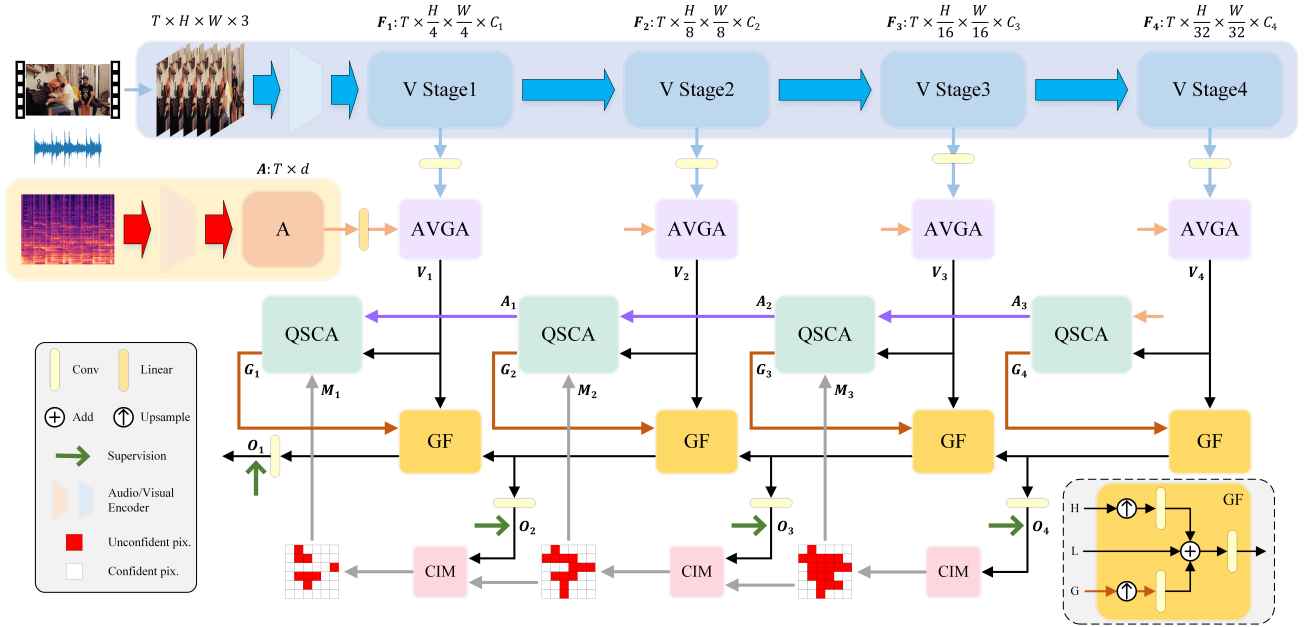


Fig. 2. Overview of the pipeline. The network takes the video clip as input and separates it into visual frames and audio spectrogram. The outputs of the audio and visual encoders are denoted as F_i and A , respectively. The features are first integrated by AVGAs and are further processed by QSCAs to generate guide features. Meanwhile, the multi-stage outputs, which are aggregated by GFs, will pass through CIMs to generate confidence masks and then be sent to QSCAs.

employs tight fusion bottlenecks to force the model to collect and condense the most relevant inputs in each modality. Sajid *et al.* [34] introduced an audio-visual Transformer and co-attention module to leverage the auxiliary patch-importance ranking and patch-wise crowd estimate information. Truong *et al.* [35] proposed another audio-visual Transformer to further exploit relationships across segments via a temporal self-attention mechanism. Lin *et al.* [36] utilized frozen ViT backbone on both audio and visual inputs by adding trainable latent hybrid adapters to attain the cross-modal association.

III. PROPOSED METHOD

A. Overview Structure of PCMANet

In this section, we introduce a novel network architecture called the Progressive Confident Masking Attention Network (PCMANet), illustrated in Figure 2. The visual frames undergo direct processing by the visual encoder, which can be either ResNet50 [37] or PVT-v2 [38], [39]. This process yields visual features denoted as F_i ($i = 1, 2, 3, 4$), where $F_i \in \mathbb{R}^{T \times h_i \times w_i \times C_i}$ and $(h_i, w_i) = (H, W)/2^{(i+1)}$. Here, T represents the number of frames. At the same time, the audio signal is converted into a mel spectrogram using a short-time Fourier transform, which is then passed through a convolutional neural network encoder, VGGish [40]. This VGG-like model is pre-trained on AudioSet [41]. The resulting output from the audio encoder is denoted as $A \in \mathbb{R}^{T \times d}$. To ensure uniformity in channel dimensions for the audio and visual features, a simple CBR (convolution, batch normalization, and ReLU) operation is applied. It regularizes all visual feature channels into $C = 256$. Similarly, a linear layer is applied to the audio feature, unifying its channel dimension to C .

In the cross-modal fusion phase, the two modal features firstly are aligned at the pixel level. They are then jointly fed into the Audio-Visual Group Attention (AVGA) modules to calculate the intrinsic correlation between the two modalities with group number g . The resulting aligned features are denoted as V_i ($i = 1, 2, 3, 4$). To further promote audio-visual information interaction, we design a Query Selection Cross Attention (QSCA) module. This module utilizes a tailored cross-attention mechanism to better capture audio cues within visual scenes. It takes the audio feature and the aligned visual features, along with an additional mask, as input. The current QSCA module produces optimized audio features denoted as A_i ($i = 1, 2, 3$), which are used in the subsequent QSCA module. Besides, the QSCA module generates enhanced visual features G_i ($i = 1, 2, 3, 4$), serving as guidance for the Guided Fusion (GF) decoder to produce corresponding outputs denoted as O_i ($i = 1, 2, 3, 4$).

Furthermore, the cross-attention operation is exceedingly computationally intensive, and the number of attention tokens can be substantial. To address this challenge, we propose a progressive Confidence-Induced Masking (CIM) unit to identify the confident pixels that should be masked and ignored during the attention computation. The mask maps are denoted as M_i ($i = 1, 2, 3$). This is the origin of the term *Query-Selected*. It directs the network's attention toward uncertain areas, typically edges, thus optimizing computational resources.

B. Audio-Visual Group Attention

With the extracted audio and visual features, it is intuitive to assess whether there exists a correlation between the audio signal and spatial localization. Previous studies[22], [18] introduced an audio-visual attention mechanism by computing the

cosine similarity between audio and visual features at the pixel level, and it was found to be effective in tasks such as sound source localization and separation. Drawing inspiration from these findings, we design a novel module named Audio-Visual Group Attention (AVGA).

As depicted in Figure 3, the process involves initially partitioning the visual features into groups, governed by a hyperparameter g , while concurrently casting the audio feature to the matching channel. Within each of these partitions, we calculate the cosine similarity by first L_2 normalizing both the audio and visual features, followed by computing the dot product of the audio feature with each pixel and summing the results along the channel axis. This procedure generates the attention map. Subsequently, the attention maps are employed to modulate the original features. Finally, a CBR operation is applied to consolidate the resulting output.

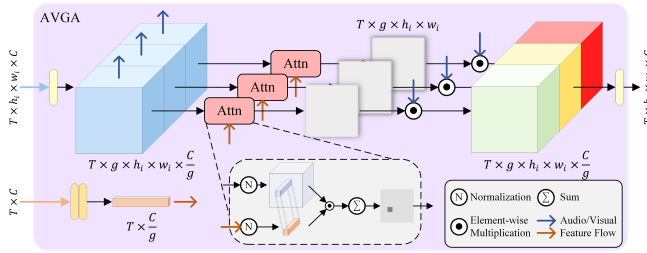


Fig. 3. Structure of Audio-Visual Group Attention (AVGA).

C. Query-Selected Cross-Attention

Following the initial fusion of audio-visual features, further information integration is necessary to unearth the mapping relationship between the audio signal and visual pixels. The Self-Attention mechanism [42], [43], a potent tool introduced by the Transformer architecture, proves highly effective in leveraging long-range dependencies among tokens, thereby addressing the challenge of local perception limitation. In the realm of multi-modal tasks, numerous endeavors have been undertaken based on the Transformer structure, spanning language-vision [44], [45], [46], [47], [48], [49], as well as audio-video [33], [17], [32], [21], [14], [24], [35], among others.

Inspired by prior research, we develop an innovative module named Query-Selected Cross-Attention (QSCA), as illustrated in Figure 4. It takes audio and visual features as inputs and produces fused audio and visual features. In contrast to similar modules, the distinctive aspect of QSCA is its audio-guided nature. Its primary objective is to identify sounding objects within the scene, with audio serving as the guiding signal. As a result, the audio output is propagated and subsequently fed into the next QSCA module, while the visual output component is utilized in the decoder to steer the generation of the segmentation map.

Furthermore, the visual tokens are redundant, and the computational cost of the attention operation is exceedingly high. To address this challenge, we propose a new query-selected mechanism. Instead of using all tokens, the network selects tokens that lack confidence for segmentation [50]. The

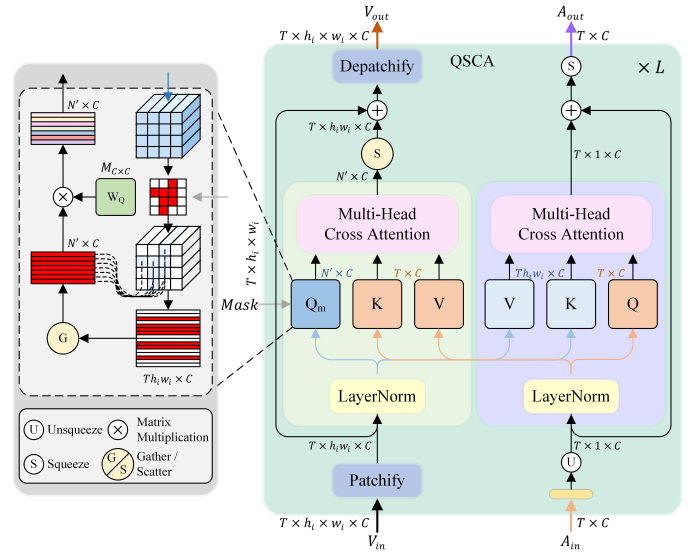


Fig. 4. Structure of Query-Selected Cross-Attention (QSCA).

criteria for selection are measured by the Confidence-Induced Masking unit (see Section III-D). The entire process can be formulated as follows: To regularize the representation, we denote $A_4 = A$, and M_4 can be considered as an all-ones matrix. Thus, the module can be represented as follows.

$$A_{i-1}, G_i = QSCA(A_i, V_i, M_i) \quad (i = 1, 2, 3, 4). \quad (1)$$

The standard attention operation can be formulated as [42]:

$$Attention(Q, K, V) = Softmax\left(\frac{QK^T}{\sqrt{d_k}}\right), \quad (2)$$

where d_k is the key's dimension.

The pipeline of QSCA can be signified as:

$$A_{i-1} = Attention(Q_a, K_v, V_v), \quad (3a)$$

$$G_i = Attention(Q_m, K_a, V_a), \quad (3b)$$

where Q_m is the query of visual features after selection. Q_x, K_x, V_x are the query, key, and the subscript x is a, v , or m .

Q_m is calculated by the following equations:

$$V_m = Gather(V_i * M_i), \quad (4a)$$

$$Q_m = V_m * W_q, \quad (4b)$$

where V_i is the visual input feature and M_i is the confident map generated by the CIM unit. W_q is the query weight matrix. $Gather(\cdot)$ is the operation that collects all the non-zero parts of the input. Following the attention operation, the $Scatter(\cdot)$ operation is employed to put the tokens back to ensure the output's shape matches the input.

Considering the gather-scatter operation, the computational cost is significantly reduced, and the least confident tokens are retained to help the network focus more effectively. To elaborate, assuming there are N tokens and C channels, for a standard Multi-Head Self-Attention (MSA), the computational complexity can be calculated as:

$$\Omega(MSA) = 4NC^2 + 2N^2C. \quad (5)$$

While for the QSCA module, denoting the masked ratio as

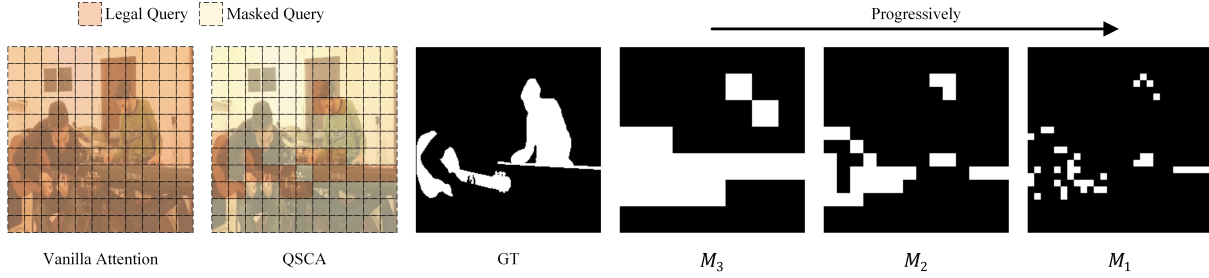


Fig. 5. An example of the QSCA and Confidence-Induced Masking (CIM).

r , we can attain the complexity formula as:

$$\Omega(\text{QSCA}) = 2NC^2 + 2N'C^2 + 2NN'C, \quad (6)$$

where $N' = rN$, the ratio r gradually increases from 0 to 1. Experiments demonstrate that in the later stages of training, r exceeds 90%, indicating that a significant portion of the tokens is masked, resulting in substantial savings in computational resources. Figure 5 provides an example of the confidence masks and the selected query.

D. Confidence-Induced Masking and Guided Fusion

To determine the confidence of each token, we propose a criterion inspired by [50]. Figure 6 illustrates the structure of this criterion. Each CIM unit takes the output O_i of each level Guided Fusion (GF) module as input. It begins by applying the *Sigmoid* function to transform the input into a prediction map. Subsequently, it employs a *Switch* operation with a hyperparameter c to assign a value of 0 (indicating background) to pixels falling within the range $[0, 1 - c] \cup [c, 1]$, which is represented in white, and a value of 1 (indicating lack of confidence) to pixels within the range $(1 - c, c)$, depicted in red. This process selects positions that are not sufficiently confident, which are then adopted for choosing tokens in the QSCA modules.

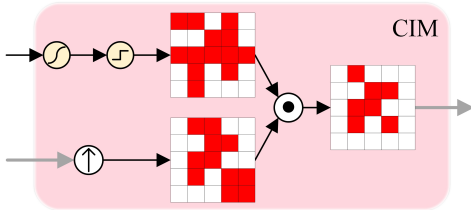


Fig. 6. Structure of Confidence-Induced Masking (CIM). Mask is generated by the output (top arrow) of current stage and previous mask (bottom arrow).

Furthermore, we desire the network to maintain prediction consistency. This implies that once a pixel is classified as confident, it should not be subsequently categorized as unconfident in later units. To achieve this, we have devised a straightforward approach. We send the previous result to the subsequent CIM's input and combine them through pixel-wise multiplication. Consequently, the confident maps exhibit consistency and progression, encouraging the network to exercise caution in its initial predictions, which can be advantageous in a progressive structure. This process can be represented by the following equation:

$$M_{i-1} = \text{CIM}(M_i, O_i). \quad (7)$$

The Guided Fusion module essentially combines adjacent features, similar to FPN [51]. The key distinction lies in its utilization of the output from the QSCA module, which has already integrated audio features. This modification ensures that the prediction generation process focuses more on the sounding objects.

IV. SUPERVISION

As we aim to regularize every confident map, we implement multi-supervision for each output O_i . For each supervision instance, we employ binary cross-entropy (BCE) and intersection over union (IoU) to compute the loss.

Binary cross entropy loss is widely adopted in segmentation tasks. It is defined as

$$\mathcal{L}_{bce} = - \sum_{(i,j)} [G_{ij} \ln P_{ij} + (1 - G_{ij}) \ln(1 - P_{ij})], \quad (8)$$

where P and G are the prediction and the ground truth label, respectively. The subscript ij refers to the pixel at (i, j) .

IoU loss evaluates the similarity between the prediction and GT from a holistic perspective rather than from a single pixel.

$$\mathcal{L}_{iou} = 1 - \frac{\sum_{(i,j)} [G_{ij} * P_{ij}]}{\sum_{(i,j)} [P_{ij} + G_{ij} - G_{ij} * P_{ij}]}. \quad (9)$$

For single supervision, the loss function is calculated by:

$$\mathcal{L}_i = \mathcal{L}_{bce}^i + \mathcal{L}_{iou}^i. \quad (10)$$

The final objective function is defined as:

$$\mathcal{L} = \sum_{i=1}^4 \lambda_i \mathcal{L}_i. \quad (11)$$

where λ_i are the hyperparameters that control the proportion of each stage's loss.

V. EXPERIMENTS

A. Datasets and Evaluation Metrics

There are three benchmark datasets: the semi-supervised Single Sound Source Segmentation (**S4**), the fully supervised Multiple Sound Source Segmentation (**MS3**), and the fully supervised audio-visual semantic segmentation (**AVSS**) [25], [26]. The S4 subset contains 4,932 videos across 23 categories, while the MS3 subset consists of 424 videos with categories selected from those in S4. These two subsets are collectively referred to as *AVSBench-object*. The train/validation/test ratio

TABLE I

QUANTITATIVE COMPARISON ON AVS DATASET. THE BEST RESULT IS HIGHLIGHTED IN RED. THE ARROW \uparrow OF THE METRICS INDICATES THE VALUE IS HIGHER THE RESULT IS BETTER. RESNET-50, PVT-v2, AND SWIN REFER TO THE RESNET-50 [37], PVT-v2 [39], AND SWIN TRANSFORMER [52], RESPECTIVELY.

Model		S4		MS3	
		$F_m\uparrow$	$mIoU\uparrow$	$F_m\uparrow$	$mIoU\uparrow$
ResNet-50	LVS	.510	37.94	.330	29.45
	3DC	.759	57.10	.503	36.92
	iGAN	.778	61.59	.544	42.89
	AVS	.848	72.79	.578	47.88
	PCMA	.858	75.24	.648	54.77
PVT-v2 / Swin	MSSL	.663	44.89	.363	26.13
	SST	.801	66.29	.572	42.57
	LGVT	.873	74.94	.593	40.71
	AVS	.879	78.74	.645	54.00
	PCMA	.893	80.10	.708	60.35

TABLE II

QUANTITATIVE COMPARISON ON AVSS DATASET. THE BEST RESULT IS HIGHLIGHTED IN RED.

Model		AVSS	
		$F_m\uparrow$	$mIoU\uparrow$
ResNet-50	3DC	.216	17.27
	AVS	.252	20.18
	PCMA	.298	24.88
PVT-v2 / Swin	AOT	.310	25.40
	AVS	.352	29.77
	PCMA	.361	31.03

for both is 70:15:15. AVSS involves a semantic segmentation task and encompasses 12,356 videos spanning 70 categories. This subset is known as *AVSBench-semantic*, with a train/validation/test split of 8,498:1,304:1,554.

Videos within the *AVSBench-object* subset are trimmed to 5 seconds ($T = 5$), whereas those within *AVSBench-semantic* are trimmed to 10 seconds ($T = 10$). Videos are equally subdivided into several 1-second clips, and labels are assigned to the frames corresponding to sounding objects. Furthermore, the supervision types differ slightly. For the S4 task, videos in the training split are only annotated for the first frame, rendering it a *semi-supervised* dataset. Conversely, for the MS3 and AVSS tasks, since sounding objects may change over time, videos in these datasets are fully annotated, making them *fully-supervised*.

We employ two metrics to assess the performance of our model and state-of-the-art methods. The mean intersection over union (**mIoU**) evaluates the similarity of the overlapped areas. The F-measure (**F_m**) [53] assesses results based on recall and precision, which can be represented as:

$$F_m = \frac{(1 + \beta^2) \cdot \text{precision} \cdot \text{recall}}{\beta^2 \cdot \text{precision} + \text{recall}}, \quad (12)$$

TABLE III

COMPLEXITY AND SPEED COMPARISON OF DIFFERENT AVS ALGORITHMS. THE RESULT OF AVS METHODS IS MEASURED BY THE DEFAULT SETTING. THE FPS TEST IS CONDUCTED ON A 16GB RAM, NVIDIA RTX4060 PC. THE BEST RESULT IS HIGHLIGHTED IN RED. THE ARROWS \uparrow (\downarrow) OF THE METRICS INDICATE THE VALUE IS HIGHER (LOWER) THE RESULT IS BETTER.

Model		Params (M) \downarrow	FLOPs (G) \downarrow	FPS \uparrow
ResNet-50	AVS	91.40	169.320	13.83
	PCMA	65.68	84.157	32.47
PVT-v2	AVS	101.32	154.137	11.63
	PCMA	94.81	107.556	18.47

where β^2 is set to 0.3.

B. Implementation Details

TABLE IV

ABLATION ANALYSIS OF PCMANET. THE BEST RESULT IS HIGHLIGHTED IN RED. THE ABBREVIATIONS "GA", "CA", AND "CI" DENOTE THE AVGA, QSCA, AND CIM MODULES, RESPECTIVELY. THE SUBSCRIPTS "M", "C", AND "P" REPRESENT "MASK", "CONTINUITY", AND "PROGRESSION", RESPECTIVELY.

Model						S4	
GA	CA _{w/o M}	CA _{w/o C}	CA	CI _{w/o P}	CI	$F_m\uparrow$	$mIoU\uparrow$
						.832	71.16
✓						.846	72.67
✓	✓					.855	74.29
✓			✓	✓		.854	74.68
✓		✓			✓	.853	74.25
✓			✓		✓	.858	75.25

In the experimental setup, we followed the methods outlined in [25], [26]. We employ two backbone architectures: ResNet-50 [37] and Pyramid Vision Transformer (PVT-v2) [38], [39] for visual feature extraction. The channel sizes for the four stages are defined as $C_{1:4} = [256, 512, 1024, 2048]$ for

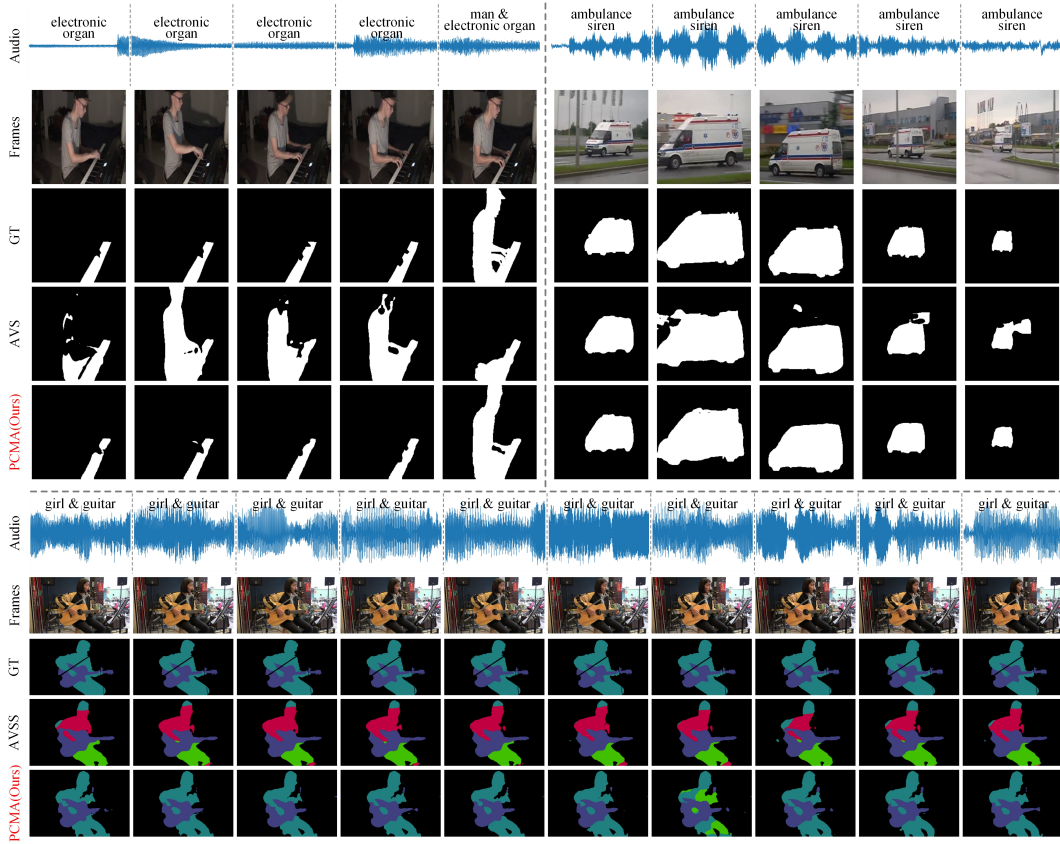


Fig. 7. Qualitative comparison among PCMANet and other AVS and AVSS methods. (Top left: MS3 task; Top right: S4 task; Bottom: AVSS task.)

ResNet-50 and $C_{1:4} = [64, 128, 320, 512]$ for PVT-v2. Audio signals are initially transformed into mel spectrograms using a short-time Fourier transform. For audio feature extraction, we utilize the VGGish[40] model, which has been pre-trained on the AudioSet [41] dataset. Visual frames are resized to dimensions of 224×224 . The unified channel size is set to $C = 256$, and the confidence threshold is configured at $c = 0.99$. The group number of AVGA is set to $g = 8$. Regarding the objective function, all λ_i values are uniformly set to 1.

During the training phase, we adopt the Adam optimizer with a learning rate of $1e-4$. The batch size is set to 4. The number of training epochs varies, with 15, 30, and 60 epochs used for the semi-supervised S4, MS3, and the AVSS tasks, respectively. These experiments are conducted on PCs equipped with 24 GB RAM and NVIDIA RTX 3090 GPUs.

C. Comparison with State of the Art Methods

1) *Quantitative Comparison*: To verify the performance of our method, we conducted a comparative analysis against the state-of-the-art algorithm, AVS [25], [26], and three other related tasks, including sound source localization (SSL), video object segmentation (VOS), and salient object detection (SOD). Specifically, we select several typical algorithms, which are LVS [28] and MSSL [27] for SSL, 3DC [54], SST[55], and AOT [56] for VOS, iGAN [57] and LGVT [58] for SOD. The quantitative results in Table I and II demonstrate

that our proposed network outperforms others, using both ResNet-50 and PVT-v2 backbones.

Furthermore, for a comprehensive evaluation, we measured the model sizes of all networks, as presented in Table III. The results highlight that PCMANet achieves superior performance with significantly reduced computational costs and faster processing speeds.

2) *Qualitative Comparison*: Figure 7 presents visualizations of the qualitative results of different AVS and AVSS algorithms. It's worth noting that all predictions were generated using the ResNet-50 backbone. As depicted in the figure, in the example of the AVSS task, our method exhibits a superior ability to capture the semantics of sounding objects while preserving their integrity. In contrast, AVS mistakenly treats different parts of a girl's colorful clothing as separate objects, failing to recognize her as a complete individual.

D. Ablation Analysis

Furthermore, we conducted ablation experiments to validate the effectiveness of the modules. For the sake of simplicity, these ablation experiments were conducted using the ResNet-50 backbone in the S4 setting.

As depicted in Figure IV, we systematically disassembled the modules to assess the impact of each individual component. In the first row, we omitted all modules, and to facilitate a fair comparison, we directly combined the audio and visual features, serving as our baseline. The "QSCA without mask"

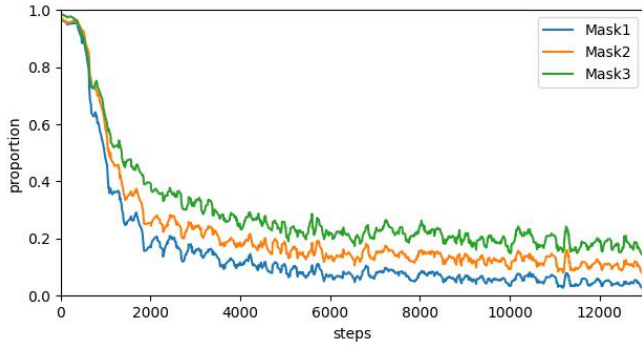


Fig. 8. Mask trends of S4 task during training phase.

condition indicates that we did not perform query selection and instead utilized all the tokens. The “QSCA without continuity” condition implies that the audio features generated from the QSCA modules were not passed to subsequent QSCA modules but remained constant using initial audio feature A . Finally, “CIM without progression” signifies that the masks calculated by the CIM units were not progressive but treated as independent. The results underscore the effectiveness of the network’s settings and modules, which are well-designed and contribute to its performance.

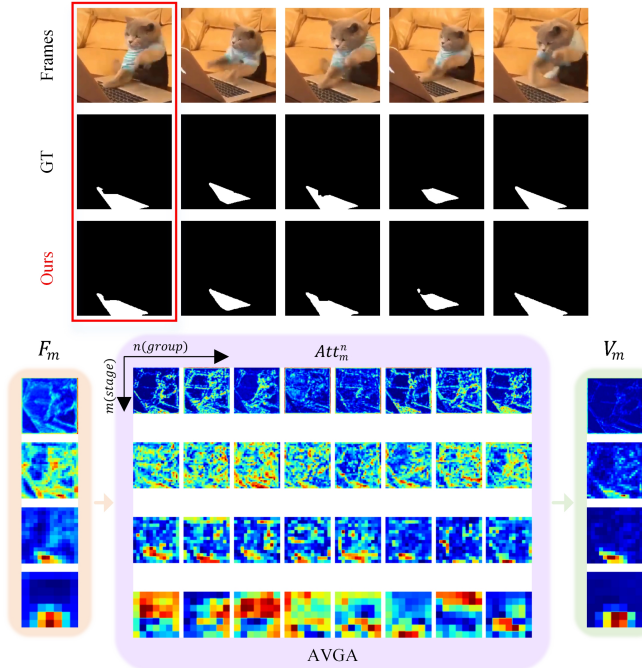


Fig. 9. Visualization of the inputs, outputs, and attention maps of AVGA module. For the sake of simplicity, the audio wave is omitted in the figure. The x and y coordinate represent m^{th} groups (from 1 to 8) and n^{th} stages (from 1 to 4), respectively.

E. Visual Analysis

In addition to the evaluation tests, we conducted several visualization experiments to further investigate the impact of

the proposed modules. All the visualization experiments are conducted on S4 task and based on ResNet-50 backbone.

Firstly, we examined the changing trend in the proportion of masked tokens within the QSCA modules, which are derived from the CIM units. Figure 8 illustrates the fluctuating proportions of the *remaining* tokens ($1 - r$) for three masks, M_i (where $i = 1, 2, 3$). It’s evident that the proportions do not increase as we move from M_1 to M_3 , aligning with the design to make the masks progressive. Moreover, during the initial training phase, the proportions drop rapidly and converge to approximately 10% (M_1) after about one-sixth of the training period. This suggests that nearly 90% of the tokens are masked after a relatively short update time, validating the efficiency and effectiveness of the modules.

Additionally, we employ visualizations of the masks to study the underlying principles of the scheme. As previously demonstrated in Figure 5, we can observe that the remaining pixels are primarily located along edges or in regions that are challenging to discern. The progressive setting ensures that the masked portion transitions from coarse, in the deep stage, to fine, in the shallow stage. Visualization demonstrates that the generated masks are both reasonable and efficient, ultimately leading to improved performance and reduced computational cost.

Finally, we delve into the AVGA modules. We denote the attention maps of AVGA as Att_m^n , where the subscript m represents the m^{th} stage ($m = 1, 2, 3, 4$), and the superscript n represents the n^{th} group ($n = 1, 2, \dots, g$). As illustrated in Figure 9, we take $g = 8$ as an example to visualize the inputs F_m , outputs V_m , and intermediate attention maps Att_m^n . For brevity, only the results for the first frame are displayed. In terms of the attention maps, different groups are capable of capturing feature similarities from various feature spaces. After passing through the AVGA module, it becomes evident that the features’ attention is concentrated on the sounding object, such as the keyboard in this instance. This result demonstrates that the AVGA module possesses the capability to locate sounding objects and learn feature similarities from different feature perspectives.

VI. CONCLUSIONS

This paper introduces the Progressive Confident Masking Attention Network (PCMANet) for the Audio-Visual Segmentation task. It leverages the Audio-Visual Group Attention (AVGA) mechanism to directly focus on the sounding region within the scene. Additionally, we explore a cross-attention scheme and design a novel Query-Selected Cross-Attention (QSCA) module to further integrate audio-visual features. Furthermore, to reduce the computational cost of the attention operation, we introduce Confidence-Induced Masking (CIM) units to mask a portion of the tokens based on the prediction confidence. Finally, we employ the Guided Fusion modules to generate the prediction maps of the network.

Sufficient experiments conducted on three benchmark AVS and AVSS datasets demonstrate the superior effectiveness of the proposed method compared to other algorithms. In the future, further investigations could focus on enhancing

performance in more complex and challenging tasks, such as AVSS.

REFERENCES

- [1] X. Zheng, X. Tan, J. Zhou, L. Ma, and R. W. H. Lau, "Weakly-supervised saliency detection via salient object subitizing," *IEEE Transactions on Circuits and Systems for Video Technology*, vol. 31, no. 11, pp. 4370–4380, 2021. **1**
- [2] M. Huang, G. Li, Z. Liu, and L. Zhu, "Lightweight distortion-aware network for salient object detection in omnidirectional images," *IEEE Transactions on Circuits and Systems for Video Technology*, vol. 33, no. 10, pp. 6191–6197, 2023. **1**
- [3] Y. Chen, G. Li, P. An, Z. Liu, X. Huang, and Q. Wu, "Light field salient object detection with location, activation and discriminative interaction network," *IEEE Transactions on Circuits and Systems for Video Technology*, vol. 34, no. 2, pp. 1070–1085, 2024. **1**
- [4] X. Jin, K. Yi, and J. Xu, "Moadnet: Mobile asymmetric dual-stream networks for real-time and lightweight rgb-d salient object detection," *IEEE Transactions on Circuits and Systems for Video Technology*, pp. 7632–7645, 2022. **1**
- [5] G. Li, Y. Wang, Z. Liu, X. Zhang, and D. Zeng, "Rgb-t semantic segmentation with location, activation, and sharpening," *IEEE Transactions on Circuits and Systems for Video Technology*, vol. 33, no. 3, pp. 1223–1235, 2023. **1**
- [6] Y. Wang, G. Li, and Z. Liu, "Sgfnnet: Semantic-guided fusion network for rgb-thermal semantic segmentation," *IEEE Transactions on Circuits and Systems for Video Technology*, pp. 7737–7748, 2023. **1**
- [7] X. Zhao, S. Chang, Y. Pang, J. Yang, L. Zhang, and H. Lu, "Adaptive multi-source predictor for zero-shot video object segmentation," in *International Journal of Computer Vision*, 2024, pp. 1573–1405. **1**
- [8] H. Zhu, M.-D. Luo, R. Wang, A.-H. Zheng, and R. He, "Deep audio-visual learning: A survey," in *International Journal of Automation and Computing*, 2021, pp. 351–376. **1**
- [9] R. Arandjelovic and A. Zisserman, "Look, listen and learn," in *Proceedings of the IEEE International Conference on Computer Vision (ICCV)*, 2017, pp. 609–617. **1, 2**
- [10] R. Arandjelovic and A. Zisserman, "Objects that sound," in *Proceedings of the European Conference on Computer Vision (ECCV)*, 2018, pp. 435–451. **1, 2**
- [11] A. Owens and A. A. Efros, "Audio-visual scene analysis with self-supervised multisensory features," in *Proceedings of the European Conference on Computer Vision (ECCV)*, 2018, pp. 631–648. **1, 2**
- [12] B. Korbar, D. Tran, and L. Torresani, "Cooperative learning of audio and video models from self-supervised synchronization," *Advances in Neural Information Processing Systems*, vol. 31, 2018. **1, 2**
- [13] Y. Tian, J. Shi, B. Li, Z. Duan, and C. Xu, "Audio-visual event localization in unconstrained videos," in *Proceedings of the European Conference on Computer Vision (ECCV)*, 2018, pp. 247–263. **1**
- [14] Y. Wu, L. Zhu, Y. Yan, and Y. Yang, "Dual attention matching for audio-visual event localization," in *Proceedings of the IEEE International Conference on Computer Vision (ICCV)*, 2019, pp. 6291–6299. **1, 2, 4**
- [15] Y.-B. Lin, Y.-J. Li, and Y.-C. F. Wang, "Dual-modality seq2seq network for audio-visual event localization," in *Proceedings of the International Conference on Acoustics, Speech and Signal Processing (ICASSP)*, 2019, pp. 2002–2006. **1**
- [16] H. Xuan, Z. Zhang, S. Chen, J. Yang, and Y. Yan, "Cross-modal attention network for temporal inconsistent audio-visual event localization," in *Proceedings of the AAAI Conference on Artificial Intelligence (AAAI)*, 2020, pp. 279–286. **1, 2**
- [17] Y.-B. Lin and Y.-C. F. Wang, "Audiovisual transformer with instance attention for audio-visual event localization," in *Proceedings of the Asian Conference on Computer Vision (ACCV)*, 2021, pp. 274–290. **1, 2, 4**
- [18] A. Senocak, T.-H. Oh, J. Kim, M.-H. Yang, and I. S. Kweon, "Learning to localize sound source in visual scenes," in *Proceedings of the IEEE Conference on Computer Vision and Pattern Recognition (CVPR)*, 2018, pp. 4358–4366. **1, 2, 3**
- [19] A. Owens, J. Wu, J. H. McDermott, W. T. Freeman, and A. Torralba, "Ambient sound provides supervision for visual learning," in *Proceedings of the European Conference on Computer Vision (ECCV)*, 2016, pp. 801–816. **1**
- [20] A. Owens and A. A. Efros, "Audio-visual scene analysis with self-supervised multisensory features," in *Proceedings of the European Conference on Computer Vision (ECCV)*, 2018, pp. 631–648. **1, 2**
- [21] Y. Cheng, R. Wang, Z. Pan, R. Feng, and Y. Zhang, "Look, listen, and attend: Co-attention network for self-supervised audio-visual representation learning," in *Proceedings of the ACM International Conference on Multimedia*, 2020, pp. 3884–3892. **1, 2, 4**
- [22] T. Afouras, A. Owens, J. S. Chung, and A. Zisserman, "Self-supervised learning of audio-visual objects from video," in *Proceedings of the European Conference on Computer Vision (ECCV)*, 2020, pp. 208–224. **1, 2, 3**
- [23] D. Hu, R. Qian, M. Jiang, X. Tan, S. Wen, E. Ding, W. Lin, and D. Dou, "Discriminative sounding objects localization via self-supervised audio-visual matching," *Advances in Neural Information Processing Systems*, pp. 10 077–10 087, 2020. **1, 2**
- [24] Y.-B. Lin, H.-Y. Tseng, H.-Y. Lee, Y.-Y. Lin, and M.-H. Yang, "Exploring cross-video and cross-modality signals for weakly-supervised audio-visual video parsing," in *Proceedings of the Conference on Neural Information Processing Systems (NIPS)*, 2021. **1, 2, 4**
- [25] J. Zhou, J. Wang, J. Zhang, W. Sun, J. Zhang, S. Birchfield, D. Guo, L. Kong, M. Wang, and Y. Zhong, "Audio-visual segmentation," in *Proceedings of the European Conference on Computer Vision (ECCV)*, 2022, pp. 386–403. **1, 5, 6, 7**
- [26] J. Zhou, X. Shen, J. Wang, J. Zhang, W. Sun, J. Zhang, S. Birchfield, D. Guo, L. Kong, M. Wang *et al.*, "Audio-visual segmentation with semantics," *arXiv preprint arXiv:2301.13190*, 2023. **1, 5, 6, 7**
- [27] R. Qian, D. Hu, H. Dinkel, M. Wu, N. Xu, and W. Lin, "Multiple sound sources localization from coarse to fine," in *Proceedings of the European Conference on Computer Vision (ECCV)*, 2020, pp. 292–308. **2, 7**
- [28] H. Chen, W. Xie, T. Afouras, A. Nagrani, A. Vedaldi, and A. Zisserman, "Localizing visual sounds the hard way," in *Proceedings of the IEEE Conference on Computer Vision and Pattern Recognition (CVPR)*, 2021, pp. 16 867–16 876. **2, 7**
- [29] S. Mo and P. Morgado, "Localizing visual sounds the easy way," in *Proceedings of the European Conference on Computer Vision (ECCV)*, 2022, pp. 218–234. **2**
- [30] B. Zhou, A. Khosla, A. Lapedriza, A. Oliva, and A. Torralba, "Learning deep features for discriminative localization," in *Proceedings of the IEEE Conference on Computer Vision and Pattern Recognition (CVPR)*, 2016, pp. 2921–2929. **2**
- [31] R. R. Selvaraju, M. Cogswell, A. Das, R. Vedantam, D. Parikh, and D. Batra, "Grad-cam: Visual explanations from deep networks via gradient-based localization," in *Proceedings of the IEEE International Conference on Computer Vision (ICCV)*, 2017, pp. 618–626. **2**
- [32] V. Iashin and E. Rahtu, "A better use of audio-visual cues: Dense video captioning with bi-modal transformer," *arXiv preprint arXiv:2005.08271*, 2020. **2, 4**
- [33] A. Nagrani, S. Yang, A. Arnab, A. Jansen, C. Schmid, and C. Sun, "Attention bottlenecks for multimodal fusion," in *Proceedings of the Annual Conference on Neural Information Processing Systems (NeurIPS)*, 2021. **2, 4**
- [34] U. Sajid, X. Chen, H. Sajid, T. Kim, and G. Wang, "Audio-visual transformer based crowd counting," in *Proceedings of the IEEE International Conference on Computer Vision Workshops (ICCVW)*, 2021, pp. 2249–2259. **3**
- [35] T.-D. Truong, C. N. Duong, T. De Vu, H. A. Pham, B. Raj, N. Le, and K. Luu, "The right to talk: An audio-visual transformer approach," in *Proceedings of the IEEE International Conference on Computer Vision (ICCV)*, pp. 1085–1094. **3, 4**
- [36] Y.-B. Lin, Y.-L. Sung, J. Lei, M. Bansal, and G. Bertasius, "Vision transformers are parameter-efficient audio-visual learners," *arXiv preprint arXiv:2212.07983*, 2022. **3**
- [37] K. He, X. Zhang, S. Ren, and J. Sun, "Deep residual learning for image recognition," in *Proceedings of the IEEE Conference on Computer Vision and Pattern Recognition (CVPR)*, 2016, pp. 770–778. **3, 6**
- [38] W. Wang, E. Xie, X. Li, D.-P. Fan, K. Song, D. Liang, T. Lu, P. Luo, and L. Shao, "Pyramid vision transformer: A versatile backbone for dense prediction without convolutions," in *Proceedings of the IEEE International Conference on Computer Vision (ICCV)*, 2021, pp. 548–558. **3, 6**
- [39] W. Wang, E. Xie, X. Li, D. Fan, K. Song, D. Liang, T. Lu, P. Luo, and L. Shao, "Pvt v2: Improved baselines with pyramid vision transformer," *Computational Visual Media*, pp. 415–424, 2022. **3, 6**
- [40] S. Hershey, S. Chaudhuri, D. P. Ellis, J. F. Gemmeke, A. Jansen, R. C. Moore, M. Plakal, D. Platt, R. A. Saurous, B. Seybold *et al.*, "Cnn architectures for large-scale audio classification," in *Proceedings of the IEEE International Conference on Acoustics, Speech and Signal Processing (ICASSP)*, 2017, pp. 131–135. **3, 7**
- [41] J. F. Gemmeke, D. P. Ellis, D. Freedman, A. Jansen, W. Lawrence, R. C. Moore, M. Plakal, and M. Ritter, "Audio set: An ontology and

- human-labeled dataset for audio events,” in *Proceedings of the IEEE International Conference on Acoustics, Speech and Signal Processing (ICASSP)*, 2017, pp. 776–780. 3, 7
- [42] A. Vaswani, N. Shazeer, N. Parmar, J. Uszkoreit, L. Jones, A. N. Gomez, L. Kaiser, and I. Polosukhin, “Attention is all you need,” in *Proceedings of the Annual Conference on Neural Information Processing Systems (NeurIPS)*, p. 11. 4
- [43] A. Dosovitskiy, L. Beyer, A. Kolesnikov, D. Weissenborn, X. Zhai, T. Unterthiner, M. Dehghani, M. Minderer, G. Heigold, S. Gelly *et al.*, “An image is worth 16x16 words: Transformers for image recognition at scale,” *arXiv preprint arXiv:2010.11929*, 2020. 4
- [44] L. H. Li, M. Yatskar, D. Yin, C.-J. Hsieh, and K.-W. Chang, “Visualbert: A simple and performant baseline for vision and language,” *arXiv preprint arXiv:1908.03557*, 2019. 4
- [45] J. Lu, D. Batra, D. Parikh, and S. Lee, “Vilbert: Pretraining task-agnostic visiolinguistic representations for vision-and-language tasks,” in *Proceedings of the Annual Conference on Neural Information Processing Systems (NeurIPS)*. 4
- [46] W. Su, X. Zhu, Y. Cao, B. Li, L. Lu, F. Wei, and J. Dai, “VI-bert: Pre-training of generic visual-linguistic representations,” *arXiv preprint arXiv:1908.08530*, 2019. 4
- [47] W. Kim, B. Son, and I. Kim, “Vilt: Vision-and-language transformer without convolution or region supervision,” in *Proceedings of the International Conference on Machine Learning*, pp. 5583–5594. 4
- [48] J. Li, R. Selvaraju, A. Gotmare, S. Joty, C. Xiong, and S. C. H. Hoi, “Align before fuse: Vision and language representation learning with momentum distillation,” in *Advances in Neural Information Processing Systems (NeurIPS)*, pp. 9694–9705. 4
- [49] J. Li, D. Li, C. Xiong, and S. Hoi, “Blip: Bootstrapping language-image pre-training for unified vision-language understanding and generation,” in *Proceedings of the 39th International Conference on Machine Learning*, pp. 12 888–12 900. 4
- [50] Z. Liu, Z. Xu, H.-J. Wang, T. Darrell, and E. Shelhamer, “Anytime dense prediction with confidence adaptivity,” *arXiv preprint arXiv:2104.00749*, 2021. 4, 5
- [51] T.-Y. Lin, P. Dollar, R. Girshick, K. He, B. Hariharan, and S. Belongie, “Feature pyramid networks for object detection,” in *Proceedings of the IEEE Conference on Computer Vision and Pattern Recognition (CVPR)*, pp. 936–944. 5
- [52] Z. Liu, Y. Lin, Y. Cao, H. Hu, Y. Wei, Z. Zhang, S. Lin, and B. Guo, “Swin transformer: Hierarchical vision transformer using shifted windows,” in *Proceedings of the IEEE international conference on computer vision*, 2021, pp. 10 012–10 022. 6
- [53] R. Achanta, S. Hemami, F. Estrada, and S. Susstrunk, “Frequency-tuned salient region detection,” in *Proceedings of the IEEE Conference on Computer Vision and Pattern Recognition (CVPR)*, 2009, pp. 1597–1604. 6
- [54] S. Mahadevan, A. Athar, A. Ošep, S. Hennen, L. Leal-Taixé, and B. Leibe, “Making a case for 3d convolutions for object segmentation in videos,” *arXiv preprint arXiv:2008.11516*, 2020. 7
- [55] B. Duke, A. Ahmed, C. Wolf, P. Aarabi, and G. W. Taylor, “Sstvos: Sparse spatiotemporal transformers for video object segmentation,” in *Proceedings of the IEEE Conference on Computer Vision and Pattern Recognition (CVPR)*, 2021, pp. 5912–5921. 7
- [56] Z. Yang, Y. Wei, and Y. Yang, “Associating objects with transformers for video object segmentation,” *Proceedings of the Annual Conference on Neural Information Processing Systems (NeurIPS)*, pp. 2491–2502, 2021. 7
- [57] Y. Mao, J. Zhang, Z. Wan, Y. Dai, A. Li, Y. Lv, X. Tian, D.-P. Fan, and N. Barnes, “Transformer transforms salient object detection and camouflaged object detection,” *arXiv preprint arXiv:2104.10127*, 2021. 7
- [58] J. Zhang, J. Xie, N. Barnes, and P. Li, “Learning generative vision transformer with energy-based latent space for saliency prediction,” *Proceedings of the Annual Conference on Neural Information Processing Systems (NeurIPS)*, pp. 15 448–15 463, 2021. 7



Yuxuan Wang is currently pursuing the M.S. degree with the Department of Computing, Imperial College London, United Kingdom. He received B.S. degrees in College of Artificial Intelligence, Nankai University. His research interests include salient object detection, computer vision, multi-modal learning, and generative model.



Feng Dong received M.S. degrees in College of Finance, Tianjin University of Finance and Economics. Her research interests include financial technology, multi-modal image analysis, and generative model.



Jinchao Zhu received the Ph.D. degree in College of Artificial Intelligence, Nankai University, China. Currently, he works as a postdoctoral scholar at BNRist, Tsinghua University. His research interests include dynamic neural network, multi-modal image/video segmentation, and diffusion model acceleration.